Soliton trapping and daughter waves in the Manakov model

D. J. Kaup
Department of Mathematics and Computer Science and Institute for Nonlinear Studies, Clarkson University, Potsdam, New York 13699-5815

B. A. Malomed
Department of Applied Mathematics, School of Mathematical Sciences, Tel Aviv University, Ramat Aviv 69978, Israel

(Received 9 November 1992)

We show that the phenomena of soliton trapping and daughter wave ("shadow") formation in optical fibers are already contained in the Manakov model [Sov. Phys. JETP **38**, 248 (1974)].

PACS number(s): 42.65.Re, 42.81.Dp, 03.40.Kf

I. INTRODUCTION

The effect of birefringence on soliton propagation in single-mode optical fibers [1,2] was first considered we believe by Menyuk [3]. This effect is an important consideration for soliton propagation because of the potential possibility of a single injected soliton being split into two separating solitons of different polarizations. Single-mode optical fibers are not really single-mode type since there exist two possible polarizations. Thus it is possible to have two modes simultaneously present, each with a different polarization. If each of these modes did propagate at the same group velocity, there would be no problem. However, optical fibers are birefringent. This means that different polarizations can have different group velocities. Thus a pulse injected into one end of an optical fiber will in general be bimodal, with each separate polarization component propagating at a slightly different velocity, eventually resulting in the separation of the two different polarizations. However, the Kerr nonlinearity can act against this tendency of bimodal pulses to split. Numerical studies by Menyuk [3] showed that there are threshold amplitudes, above which the bimodal soliton would not split (the unsplit two-component soliton is frequently called a vector soliton). This phenomenon of bimodal solitons being forced to propagate together in a birefringent materials has been termed "soliton trapping." Theoretical studies of soliton trapping have been done by Ueda and Kath [4] where they used a variational principle to study the interacting modes, while Kivshar [5] has studied the phenomenon from the point of view of the interaction energy between the trapped solitons. All these studies confirm that soliton trapping does occur and they also give threshold values for trapping to occur.

Another phenomenon observed in numerical studies is the formation of "shadows" [6] which are small daughter pulses that split off from a soliton and propagate along beside it in the other mode. This effect has been studied in some detail numerically [4]. An analytical approach based on the perturbation theory has been developed recently in Ref. [9].

What we will show here is that, to a certain extent, both the birefringence-induced splitting of an initial vector pulse and the formation of the "shadows" are already contained in the well-known integrable model proposed by Manakov [7] in 1973. Due to the vector nature of the electric field, the cross-coupling coefficient for linearly polarized pulses in optical fibers is $\frac{2}{3}$ whereas in the Manakov model it is unity. Thus the Manakov model has one coefficient off by 30% and slightly overestimates the strength of the cross coupling. However, we argue that even so, in any reasonable sense, the Manakov model is still "close" to the actual physical model for linearly polarized pulses and a study of the Manakov model would at least give a qualitative understanding of what is happening, and perhaps even quantitatively also. In fact we find a wealth of information in the Manakov model. We can delineate threshold regimes for decay, soliton trapping, soliton splitting, and even soliton-shadow formation. While the quantitative values could be questioned because of the unity value of the cross coupling, nevertheless the qualitative regimes that we find do agree with what is observed numerically. Of course, as shown by Menyuk [6], the cross-coupling coefficient is quite sensitive to the modal nature of the birefringence. If the birefringence is elliptical ($\theta \simeq 35°$), then the cross-coupling coefficient would be exactly unity with our results here being essentially quantitatively correct as well (except for the profile shape).

So, the Manakov model does prove to be quite useful in giving, at least, a qualitative understanding of all these phenomena. To achieve a better quantitative description of the linearly polarized birefringence, one could take advantage of the fact that the above-mentioned value of the cross-coupling coefficient, $\frac{2}{3}$, is rather close to Manakov's value of 1. Then, one could develop a variant of the perturbation theory using Manakov's model as the zeroth-order approximation. This approach, developed in Refs. [9–11], seems to be promising. However, the idea that we pursue in this present work is very simple. The main point is to solve the so-called direct scattering problem for an initial profile of the vector pulse in the Manakov system. Actually, we do this for the box-shaped initial pulse, which is easiest to solve (but which, nevertheless, yields quite nontrivial results). The eigenvalues and the

associated normalization coefficients that characterize the discrete components of the spectrum generated by the solution of the direct scattering problem contain full information about the soliton content of the initial pulse.

II. THE INITIAL-VALUE PROBLEM

The governing equations for bimodal propagation in a birefringent optical fiber are

$$i(\partial_x u+\delta\partial_t u)+\tfrac{1}{2}\partial_t^2 u+(u^*u+\epsilon v^*v)u=0\ , \tag{1a}$$

$$i(\partial_x v-\delta\partial_t v)+\tfrac{1}{2}\partial_t^2 v+(v^*v+\epsilon u^*u)v=0\ , \tag{1b}$$

where u and v are the normalized envelopes of the two modes, t and x are the normalized time and distance along the fiber, ϵ is the cross-coupling coefficient (which is unity in the Manakov model and $\frac{2}{3}$ in a linear birefringent optical fiber), and δ is one-half of the velocity splitting due to birefringence. By the simple phase transformation [4]

$$u=q_1\exp\left[i\frac{\delta^2}{2}x-i\delta t\right]\ , \tag{2a}$$

$$v=q_2\exp\left[i\frac{\delta^2}{2}x+i\delta t\right]\ , \tag{2b}$$

one can transform away the birefringence in (1), giving

$$i\partial_x q_1+\tfrac{1}{2}\partial_t^2 q_1+(q_1^*q_1+\epsilon q_2^*q_2)q_1=0\ , \tag{3a}$$

$$i\partial_x q_2+\tfrac{1}{2}\partial_t^2 q_2+(q_2^*q_2+\epsilon q_1^*q_1)q_2=0\ . \tag{3b}$$

However, the effects of the birefringence have not been eliminated but have simply been transferred to the initial data. If at $x=0$, $u(t,x=0)$ and $v(t,x=0)$ are proportional, then by (2), $q_1(t,x=0)$ and $q_2(t,x=0)$ will be proportional only in their amplitudes, with each having an oppositely directed phase. Thus the effect of the birefringence can be transferred to the phasing of the initial data.

When the cross-coupling coefficient ϵ is unity, (3) is integrable [7] and can be solved by an inverse scattering transform (IST). The necessary Lax pair [7] is

$$v_{1t}+i\zeta v_1=q_1v_2+q_2v_3\ , \tag{4a}$$

$$v_{2t}-i\zeta v_2=-q_1^*v_1\ , \tag{4b}$$

$$v_{3t}-i\zeta v_3=-q_2^*v_1\ , \tag{4c}$$

and

$$i\partial_x v_1=[\zeta^2-\tfrac{1}{2}(q_1^*q_1+q_2^*q_2)]v_1+[i\zeta q_1-\tfrac{1}{2}\partial_t q_1]v_2+[i\zeta q_2-\tfrac{1}{2}\partial_t q_2]v_3\ , \tag{5a}$$

$$i\partial_x v_2=[-i\zeta q_1^*-\tfrac{1}{2}\partial_t q_1^*]v_1+[-\zeta^2+\tfrac{1}{2}q_1^*q_1]v_2+\tfrac{1}{2}q_1^*q_2v_3\ , \tag{5b}$$

$$i\partial_x v_3=[-i\zeta q_2^*-\tfrac{1}{2}\partial_t q_2^*]v_1+\tfrac{1}{2}q_1q_2^*v_2+[-\zeta^2+\tfrac{1}{2}q_2^*q_2]v_3\ , \tag{5c}$$

where ζ is the spectral parameter. Since (3), for $\epsilon=1$, is the integrability condition for a common solution of (4) and (5) to exist, then we may solve (3) by solving (4) and (5) instead. To do this, we determine the scattering data of (4) and determine its x evolution with (5). One may define the scattering data from the scattering coefficients. These are defined as follows [7]. First assume that q_1 and q_2 are integrable with respect to t. Let $\Phi(\zeta,x)$ be the solution matrix for (4) subject to the boundary condition

$$\Phi(\zeta,x\to-\infty)=\begin{bmatrix}e^{-i\zeta x}&0&0\\0&e^{i\zeta x}&0\\0&0&e^{i\zeta x}\end{bmatrix}\ . \tag{6}$$

Then as $x\to+\infty$, we will have

$$\Phi(\zeta,x)\to\begin{bmatrix}e^{-i\zeta x}&0&0\\0&e^{i\zeta x}&0\\0&0&e^{i\zeta x}\end{bmatrix}S^T\ , \tag{7}$$

where T indicates the matrix transpose and S is the 3×3 matrix of scattering coefficients a_{ij} where

$$S=[a_{ij}]\ . \tag{8}$$

One can show [7] that the matrix S is unitary for real ζ,

$$S^\dagger S=I\ . \tag{9}$$

From (5), it follows [7] that the x evolution of S is given by

$$\partial_x S=i\zeta^2[J,S]\ , \tag{10}$$

where J is the diagonal matrix

$$J=(+,-,-)\ . \tag{11}$$

The scattering data for inversion about $+\infty$ consists of the continuous spectra $[\rho_1(\zeta)=a_{12}(\zeta)/a_{11}(\zeta)$ and $\rho_2(\zeta)=a_{13}(\zeta)/a_{11}(\zeta)$ for ζ real] and a bound-state spectrum. The latter consists of the zeros of $a_{11}(\zeta)$ for ζ in the upper half complex plane and a set of normalization coefficients (C_1,C_2) for each bound state. Let N be the total number of bound states and ζ_n $(n=1,2,\ldots,N)$ be the zeros of $a_{11}(\zeta)$ in the upper half plane. Then the normalization coefficients (the residues of the ρ's) are

$$C_{1n}=\frac{a_{12}(\zeta_n)}{a_{11}'(\zeta_n)}\ , \tag{11a}$$

$$C_{2n}=\frac{a_{13}(\zeta_n)}{a_{11}'(\zeta_n)}\ , \tag{11b}$$

where a_{11}' is the derivative of $a_{11}(\zeta)$ with respect to ζ. From (10) it follows that for real ζ

$$\partial_x a_{11}(\zeta)=0\ , \tag{12a}$$

$$\partial_x\rho_1=2i\zeta^2\rho_1\ , \tag{12b}$$

$$\partial_x\rho_2=2i\zeta^2\rho_2\ , \tag{12c}$$

and for the bound-state parameters

$$\partial_x \zeta_n = 0 , \tag{12d}$$

$$\partial_x C_{1n} = 2i\zeta_n^2 C_{1n} , \tag{12e}$$

$$\partial_x C_{2n} = 2i\zeta^2 C_{2n} . \tag{12f}$$

The solution of the initial value problem consists of simply solving (4) for the scattering data at $x=0$ by using the initial profiles for q_1 and q_2. Then by (12) one can determine the scattering data at any later position. Now one uses the inverse scattering equations to reconstruct q_1 and q_2 at any later x. The inverse scattering equations are [7]

$$F_1(\zeta) = \begin{bmatrix} 1 \\ 0 \\ 0 \end{bmatrix} + \frac{1}{2\pi i} \int_C \frac{d\zeta'}{\zeta' - \zeta} e^{2i\zeta' t} \times [\rho_1(\zeta') F_2(\zeta') + \rho_2(\zeta') F_3(\zeta')] , \tag{13a}$$

$$F_2(\zeta) = \begin{bmatrix} 0 \\ 1 \\ 0 \end{bmatrix} + \frac{1}{2\pi i} \int_{\bar{C}} \frac{d\zeta'}{\zeta' - \zeta} e^{-2i\zeta' t} \rho_1^*(\zeta') F_1(\zeta') , \tag{13b}$$

$$F_3(\zeta) = \begin{bmatrix} 0 \\ 0 \\ 1 \end{bmatrix} + \frac{1}{2\pi i} \int_{\bar{C}} \frac{d\zeta'}{\zeta' - \zeta} e^{-2i\zeta' t} \rho_2^*(\zeta') F_1(\zeta') , \tag{13c}$$

where C is the contour in the complex plane above all zeros of $a_{11}(\zeta)$ [the poles of $\rho_1(\zeta)$ and $\rho_2(\zeta)$] while $\bar{C}$ is its mirror image in the lower half complex plane. Lastly, one can recover q_1 and q_2 from the following asymptotic limit for large ζ:

$$(0,\alpha,\beta) F_1|_{\zeta \to \infty} = \frac{1}{2i\zeta} (\alpha q_1^* + \beta q_2^*) \tag{14}$$

for any values of α and β, or

$$(1,0,0) F_2|_{\zeta \to \infty} = \frac{1}{2i\zeta} q_1 , \tag{15a}$$

$$(1,0,0) F_3|_{\zeta \to \infty} = \frac{1}{2i\zeta} q_2 . \tag{15b}$$

Of the above parts, we are only interested in the bound-state part (the discrete component of the spectrum) which determines the soliton content of the solution. The continuous spectrum will always dispersively decay and is of no interest since after any reasonably short distance it will be gone. What will be left will be only the solitons. In this case only the poles contribute to (13), which reduces to

$$F_1(\zeta) = \begin{bmatrix} 1 \\ 0 \\ 0 \end{bmatrix} - \sum_{n=1}^{N} \frac{e^{2i\zeta_n t}}{\zeta_n - \zeta} [C_{1n} F_2(\zeta_n) + C_{2n} F_3(\zeta_n)] , \tag{16a}$$

$$F_2(\zeta) = \begin{bmatrix} 0 \\ 1 \\ 0 \end{bmatrix} + \sum_{n=1}^{N} \frac{e^{-2i\zeta_n^* t} C_{1n}^*}{\zeta_n^* - \zeta} F_1(\zeta_n^*) , \tag{16b}$$

$$F_3(\zeta) = \begin{bmatrix} 0 \\ 0 \\ 1 \end{bmatrix} + \sum_{n=1}^{N} \frac{e^{-2i\zeta_n^* t} C_{2n}^*}{\zeta_n^* - \zeta} F_1(\zeta_n^*) , \tag{16c}$$

which are a set of linear nonhomogeneous algebraic equations.

The only solutions of (16) that will be of interest to us are the one- and two-soliton solutions. For the one-soliton solution, (12), (15), and (16) give

$$q_1 = \frac{2\eta_1 \epsilon_1 \exp\{2i[(\xi_1^2 + \eta_1^2)x - \xi_1(t - t_0 + 2\xi_1 x)]\}}{\cosh[2\eta_1(t - t_0 + 2\xi_1 x)]} , \tag{17a}$$

$$q_2 = \frac{2\eta_1 \epsilon_2 \exp\{2i[(\xi_1^2 + \eta_1^2)x - \xi_1(t - t_0 + 2\xi_1 x)]\}}{\cosh[2\eta_1(t - t_0 + 2\xi_1 x)]} , \tag{17b}$$

where

$$\zeta_1 = \xi_1 + i\eta_1 , \tag{18}$$

$$C_1 = -2i\eta_1 \epsilon_1^* e^{2\eta_1 t_0} e^{-2i\xi_1 t_0} , \tag{19a}$$

$$C_2 = -2i\eta_1 \epsilon_2^* e^{2\eta_1 t_0} e^{-2i\xi_1 t_0} , \tag{19b}$$

$$\epsilon_1^* \epsilon_1 + \epsilon_2^* \epsilon_2 = 1 . \tag{20}$$

One notes that the real part of the eigenvalue gives us the soliton velocity while the imaginary part gives the amplitude and width. The ratio of C_1/C_2 gives the relative sizes of the two modes while the total amplitude, $C_1^* C_1 + C_2^* C_2$, gives the central position.

The two-soliton solution is more complex, but when the two solitons have a relative separation larger than their combined widths, the solution approaches a sum of the one-soliton solutions. For the leading soliton, the values of t_0, ϵ_1, and ϵ_2 will be correct but for the lagging soliton, there will be a shift in t_0 as well as a rotation of the polarization (ϵ_1, ϵ_2). These corrections would be necessary for any quantitative comparisons.

III. RESULTS FOR BOX PROFILES

The easiest case to analyze would be for initial boxlike profiles where q_1 and q_2 are zero for $t > 0$ or $t > 1$ and in between

$$q_1 = Qe^{ikt} , \tag{21a}$$

$$q_2 = Qe^{-ikt} , \tag{21b}$$

where Q and k are constants. Menyuk [3] and others [4,5] have used the typical sech(t) shape. Our justification for the boxlike profile is that (4) can be reduced to the constant coefficient case, allowing an algebraic solution which can be rapidly numerically calculated. Also, for areas larger than $\pi/2$, the radiation component of the box profile is relatively small and the eigenvalue spectrum is not too different from that of other profiles [8].

Taking (21) to be the initial profiles, we fix Q and k, then choose a value for ζ. From the algebraic solution,

we calculate the general matrix S as given in (7). We first calculate the phase of a_{11} along the real ζ axis to determine the number of bound states. Then we calculate $a_{11}(\zeta)$ on a course grid in the upper half complex ζ plane to localize the approximate position of each zero. Then a Newton method is used to converge onto the exact location of the zero, at which the values of C_1 and C_2 are calculated. Then we repeat the above procedures for other values of Q and k. The results for the bound-state eigenvalues are shown in Figs. 1 and 2. In Fig. 1 we plot the imaginary parts, η_n, versus the birefringence factor k for various areas (simply Q). For the initial profiles (21), we have an initial pulse polarized at 45°. Along with the direction of polarization, the pulse has an amplitude of $\sqrt{2}Q$ and an area of the same amount (for $k=0$). Now the critical area when $k=0$ for soliton formation is $\pi/2$, so the first soliton will appear when $Q=\pi/2^{3/2}=1.11$. However, this soliton would have a zero amplitude. So we choose $Q=1.5$ as our first curve. One observes that for this value of Q we obtain a rather small value for $\eta_1=0.81$, which soon drops to even smaller values as k increases, vanishing at $k=2.1$, with no other solitons possible for larger values of k.

There is another critical area that one has to keep in mind and that is if $Q>\pi/2=1.57$, then it is possible to have separating solitons, one in each mode. That does not happen for $Q=1.5$ because we are just below the threshold for the generation of individual separating solitons in each mode. However, for $Q=1.8$, we are above that threshold. At $k=0$, we have only one mixed-mode soliton with $\eta_1=1.38$ (the threshold for two solitons at $k=0$ is $\sqrt{2}Q=3\pi/2$ or $Q=3.33$). As k increases, this η_1 decreases until it vanishes between $k=2.4$ and 2.5. Between $k=2.5$ and 2.8, there are no solitons produced, but above $k=2.8$ we have two separating solitons. What has happened here is that the initial relative velocity between the two modes is now sufficient for each mode to rapidly pass through the other, thereby quickly separating and since each mode has a sufficient area ($Q>\pi/2$), a single soliton is generated for each mode. From Fig. 2, one can see that the relative velocity of separation quickly becomes proportional to k. Above $Q=1.8$, for any k there is always at least one soliton produced. For $Q=2.0$, between $k=0$ and approximately 2.6, there is only one mixed-mode (trapped) soliton produced. At approximately $k=2.6$, there is a bifurcation where another zero of a_{11} rapidly rises up from below the real axis and joins the other zero which is falling down. Then they split into two separating single-mode (escaping) solitons. This second zero which rises up from below cannot be seen at $Q=2.0$ or 2.2 because of the extremely small range of k in which it exists. However, for $Q=2.8$ or 3.3, it is more easily seen since it then exists over a much wider range of k. This second mixed-mode soliton will appear as a "shadow" of the main (larger) soliton since it also has a purely imaginary eigenvalue, therefore moving parallel with the main soliton. As we shall see later, it also lags behind the main soliton. One observes that for $Q=3.3$ this shadow soliton is almost ready to appear at $k=0$. This is because the $k=0$ threshold for two mixed-mode solitons is $\sqrt{2}Q=3\pi/2$, or $Q=3.33$ as mentioned earlier. Above this value of Q, we are in the range where multiple soliton production would occur. Since multiple solitons are not desirable in optical communication, we have stopped at $Q=3.3$.

From these data we can construct Fig. 3, which shows the regions for soliton trapping, escaping, decaying, and shadow formation. If no solitons are produced, we have only decaying continuous spectra (radiation) which are the lower part of Fig. 3. Above this and to the left is the region of soliton trapping. Here one will at first only obtain a single mixed-mode soliton, but when Q becomes larger than about 2.5 or so, one will also obtain a second mixed-mode shadow soliton. To the right is the region where solitons will not be trapped. Rather they will escape and separate into two single-mode solitons. One should note the general shape of the trapping region. It is bounded from below by the threshold for mixed-mode

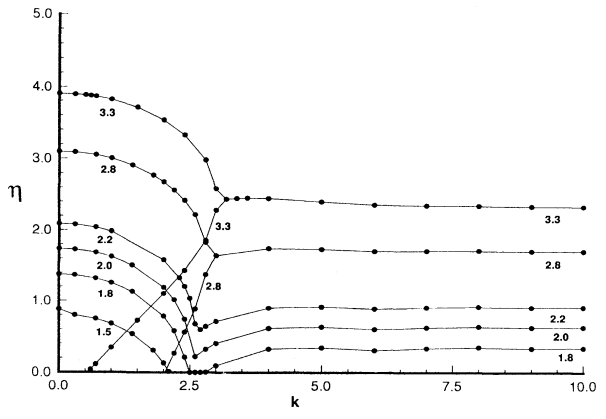

FIG. 1. Plots of the imaginary part of the bound-state eigenvalues η vs the birefringence factor k for various initial pulse areas from 1.5 to 3.3. The dots are the numerical values obtained.

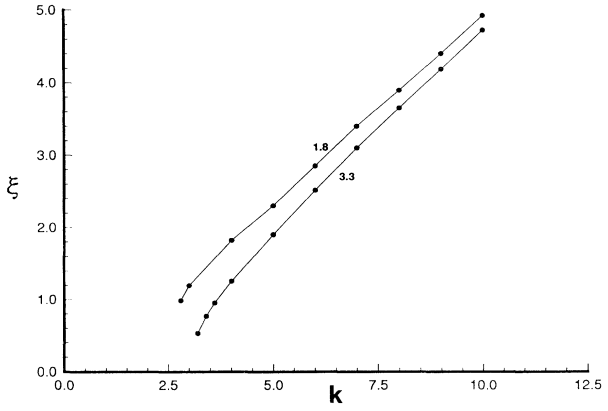

FIG. 2. Plots of the real part of the bound-state eigenvalues vs the birefringence factor k for initial pulse areas of 1.8 and 3.3. The curves for other areas basically lie between these two curves.

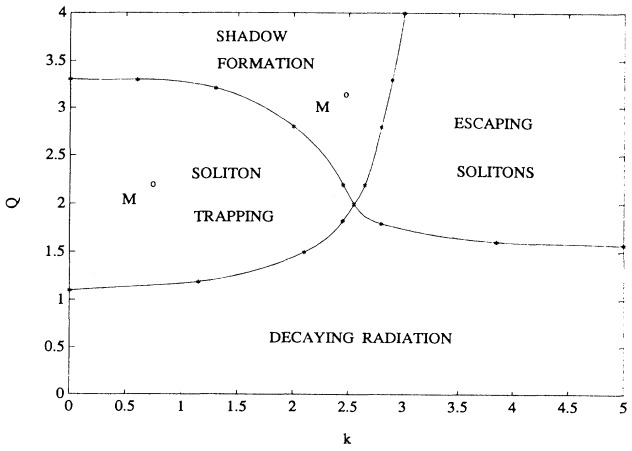

FIG. 3. Plot of the regions for soliton trapping, shadow production, escaping solitons, and the region where only decaying radiation is produced. The two points labeled M are the data points obtained by Menyuk [3] in his numerical studies. The vertical axis is the initial area and the horizontal axis is the birefringence factor k.

soliton production and to the right by $k \approx 2.8$. This suggests that there is probably an upper limit to k for soliton trapping of $k \approx 3.0$. If the birefringence factor is larger than this, one may never see soliton trapping.

We now make some comments on the relative positions and polarizations of these solitons. The position of a soliton is strongly affected by its height as one can see in (19). In general, C_1 and C_2 will always be some nonzero value. Thus we have

$$t_0 = \frac{1}{4\eta_1} \ln \left[\frac{C_1^* C_1 + C_2^* C_2}{4\eta_1^2} \right] . \tag{22}$$

Clearly, if η_1 is small and in particular as $\eta_1 \to 0$, we see that t_0 will take on large and positive values. This means that small-amplitude solitons will take long times to form and will, in general, follow behind any larger solitons. Thus the shadow solitons, usually in general of small amplitudes, will indeed follow behind the main soliton. For example, when a soliton has an amplitude of less than $\frac{1}{10}$, in general t_0 will be of order 10 or more since C_1 and C_2 are typically of order unity. This means that shadow solitons will usually be several or many widths behind the main soliton. This also creates difficulty in observing such solitons in numerical calculations since a very long grid would have to be used in order to allow them to have time to form.

The polarization of the resulting unsplit vector solitons was found, as one would expect for our symmetric initial state, to always be at 45°. But the escaping solitons were not the pure polarized (single-mode) solitons. For large k, they do asymptotically approach pure single-mode solitons but would typically have a few percent of the other mode present. Near the bifurcation point, the mixture could be much larger, but only very near this point.

Let us now compare these results with the numerical observations of Menyuk [3]. There are four differences to consider. First, there are the differences in the profile shapes. He used $q = A\ \mathrm{sech}(t)$ which at $k = 0$ has an area of πA and an energy $E = \int_{-\infty}^{\infty} q^* q dt$ of $2A^2$. Our box profile has an area of Q and an energy of Q^2. Since the nonlinear Schrödinger equation (NLS) is scale invariant, we can compare scale invariants. Two invariants are the area and the ratio of the energy to the birefringence factor, E/k. Doing so, we can take his threshold values and plot them in Fig. 3. These are the points labeled M in Fig. 3. As one can see, they lie above our threshold curve. The second difference is the mixed-mode coupling constant, ϵ in Eq. (3). He used $\frac{2}{3}$ and we used unity. This means that the effective nonlinearity of the mixed mode for $\epsilon = \frac{2}{3}$ is less than that for $\epsilon = 1$. Thus if he had used $\epsilon = 1$ instead of $\epsilon = \frac{2}{3}$, his threshold would have been smaller by some factor. Simply scaling the nonlinearity suggests that this factor would be $\sqrt{5/6}$, which would reduce his values by only about 10%. A third factor is the ability to observe the actual threshold. At the threshold, one only produces a zero-amplitude soliton. One could not observe a zero-amplitude soliton numerically. Furthermore, just above threshold, the soliton will have a very low amplitude, and will take a very long time to form. Thus it would be relatively indistinguishable from the continuous spectra dispersing away. On the other hand, our analytical results can pinpoint precisely when a zero-amplitude soliton forms. Thus any numerically observed threshold would always lie above the analytically observed threshold. Fourth and last, we have used an integrable model whereas for $\epsilon = \frac{2}{3}$ the model is nonintegrable. In any nonintegrable theory, solitons (actually solitary waves instead) can interact and can gain and lose energy in collisions with each other. In particular, during formation as in an initial-value problem such as this, one would expect that solitary wave formation would tend to pump energy into the continuous spectra, particularly if the initial modes were predominantly solitary waves, simply because there is a low intensity of continuous spectra present for providing energy to the solitary waves. Thus one would expect the threshold for a nonintegrable model to be higher than that for a similar integrable model.

Nevertheless, even with these differences, we see that the Manakov model can provide valuable insight into the phenomena of soliton trapping, decaying, and escaping, and it can help to delineate the regions of each. The quantitative values might be off somewhat, but the qualitative picture does seem to be very good. Even for the problem of the shadow formation, this exactly solvable model yields useful results. However, it should be noted that the latter problem can be formulated in its full form only within the framework of nonintegrable models, since there is a rigorous result that a collision of two solitons with strictly orthogonal polarizations in the Manakov system can never change their polarizations. At the same time, the perturbation theory based on the Manakov system was effectively applied in Ref. [9] just to the problem of the collision-induced shape formation, and it seems plausible that this version of the perturbation theory can find more applications. This issue will be considered elsewhere.

ACKNOWLEDGMENTS

This work was sponsored in part by the Office of Naval Research through Grant No. N00014-91-J-1332 and the Air Force Office of Scientific Research through URI Grant No. F49620-93-1-0088.

[1] A. Hasegawa and F. Tappert, Appl. Phys. Lett. **23**, 142 (1973).
[2] L. F. Mollenauer, R. H. Stolen, and J. P. Gordon, Phys. Rev. Lett. **45**, 1045 (1980).
[3] C. R. Menyuk, Opt. Lett. **12**, 614 (1987).
[4] T. Ueda and W. L. Kath, Phys. Rev. A **42**, 563 (1990).
[5] Y. S. Kivshar, J. Opt. Soc. Am. B **7**, 2204 (1990).
[6] C. R. Menyuk, IEEE J. Quantum Electron. **QE-23**, 174 (1987); Opt. Lett. **12**, 614 (1987); IEEE J. Quantum Electron. **QE-25**, 2674 (1989).
[7] S. V. Manakov, Zh. Eksp. Teor. Fiz. **65**, 505 (1973) [Sov. Phys. JETP **38**, 248 (1974)].
[8] D. J. Kaup, Phys. Rev. A **16**, 704 (1977).
[9] B. A. Malomed, J. Opt. Soc. Am. (to be published).
[10] D. J. Muraki and W. L. Kath, Phys. Lett. A **139**, 379 (1989).
[11] B. A. Malomed, Phys. Rev. A **43**, 410 (1991).